Applied Physics A (2018) 124:181
https://doi.org/10.1007/s00339-018-1607-4

Applied Physics A
Materials Science & Processing

Mechanisms of damage formation in glass in the process of femtosecond laser drilling

Yusuke Ito[1] · Rin Shinomoto[1] · Keisuke Nagato[1] · Akinori Otsu[1] · Kentaro Tatsukoshi[2] · Yasuji Fukasawa[2] · Toru Kizaki[1] · Naohiko Sugita[1] · Mamoru Mitsuishi[1]

Received: 18 October 2017 / Accepted: 22 January 2018 / Published online: 27 January 2018

Abstract
The development of femtosecond lasers has renovated micromachining technology, enabling the microdrilling of transparent materials at high speed. Although effective, this technique is still imperfect because irregular microscopic damage occurs during processing. Several factors in the formation of damage induced by a single laser pulse have been suggested; however, the entire mechanisms of damage formation in the process of drilling are not fully understood. Here we investigated the causes of microscopic damage both by experimentally carrying out laser drilling on chemically strengthened glass samples and by numerically analyzing the propagating stress wave and temperature distribution. We have revealed that the damage at the sidewall and bottom of a generated hole is mainly due to the stress wave, while the damage around the hole entrance is mainly due to relaxation of thermal stress. In particular, we have analyzed these processes quantitatively, demonstrating the time courses of the passage of the stress wave through the material and the temperature distribution generated by the excited electrons. Our analyses are useful in suggesting processing techniques, or suggesting glass materials suitable for laser drilling such as glass with high heat resistance, which may lead to an improvement in the quality of micromachining.

1 Introduction

The development of femtosecond laser technology has brought about changes in a variety of applications, including the microdrilling of materials [1, 2]. Thereby, the use of the femtosecond laser has already become an essential technology in micromachining [3–6]. Nevertheless, the laser drilling of glass is still imperfect, mainly because precision processing is impaired by the irregular microscopic damage that occurs during drilling [7]. This unwanted damage occurs as a by-product of the ablation of the material due to high-intensity laser pulses. The main factors contributing to the individual types of damage caused by a single laser shot have been studied extensively [8–16]; the shock originating from the photoexcited region generates microscopic cracks, while the high heat leads to modifications in the material. Meanwhile, the damage caused by repeated application of laser beams has been investigated mainly from the aspect of excited electrons [17, 18]. Conversely, the damaging effects of shock and high heat during drilling have not been fully researched. We investigated the dependence of damage on the stress field by conducting experiments, and estimated the contributions of shock and heat on the damage formation separately by performing numerical analyses on the propagating stress wave and the temperature distribution.

2 Experimental

The experiments of femtosecond laser drilling were conducted both before and after chemically strengthening glass samples. The induced compressive stress on the surface layer of glass was 359 MPa. The depth of the compressive-stress layer was 62 µm, and the deeper area has a tensile-stress field with the maximum stress of 39.2 MPa. A Yb:KGW laser system was used to generate femtosecond laser pulses with a central wavelength of 514 nm, pulse width of 228 fs, and repetition rate of 1 kHz. The pulse energy was 60 µJ and the spot diameter was 9.6 µm. The experimental setup and

✉ Yusuke Ito
y.ito@mfg.t.u-tokyo.ac.jp

Kentaro Tatsukoshi
kentaro-tatsukoshi@agc.com

[1] Department of Mechanical Engineering, School of Engineering, The University of Tokyo, Bunkyo, Tokyo 113-8656, Japan

[2] AGC Asahi Glass, Yokohama 230-0045, Kanagawa, Japan

the stress distribution in the chemically strengthened glass sample are shown in Fig. 1.

3 Results and discussion

3.1 Damage generated inside glass

Figure 2 shows the images of holes drilled on glass samples with 75 and 130 laser pulses. Background subtraction was conducted after recording images with an optical microscope. The dashed line shown in Fig. 2 represents the border between the regions of compressive and tensile stress.

Figure 2a shows that the damage around the sidewall and the bottom of the hole was inhibited in the compressive-stress region. However, when the depth of the hole approached the tensile-stress region, the damage at the bottom of the hole expanded as shown in Fig. 2b.

In addition to the damage around the sidewall and the bottom of the hole, damage was found at the entrance of the hole, as shown in Fig. 2c. However, Fig. 2a, b shows that the damage around the entrance was not inhibited in the compressive-stress region.

Figure 3 shows the results obtained with a various number of laser pulses. Figure 3a shows the dependence of the depth of a hole on the number of pulses. The dependence of

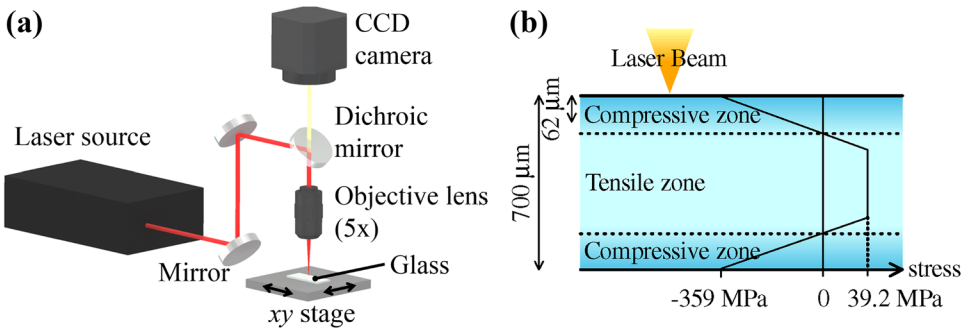

Fig. 1 **a** Experimental setup. **b** Stress distribution in chemically strengthened glass

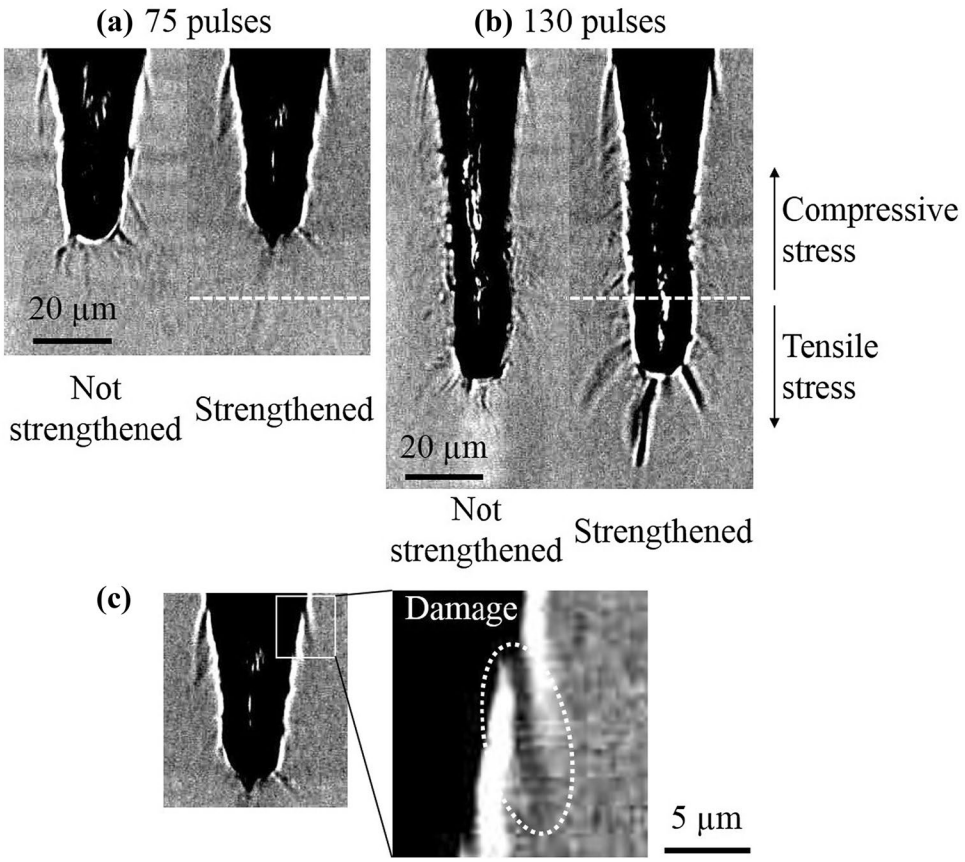

Fig. 2 Images of drilled holes taken by an optical microscope. Holes drilled by **a** 75 laser pulses and **b** 130 laser pulses. Images on the left and right in (**a**) and (**b**) show the holes drilled on glass before and after chemically strengthening, respectively. **c** Magnified view of the damage around the entrance of the hole drilled by 75 laser pulses

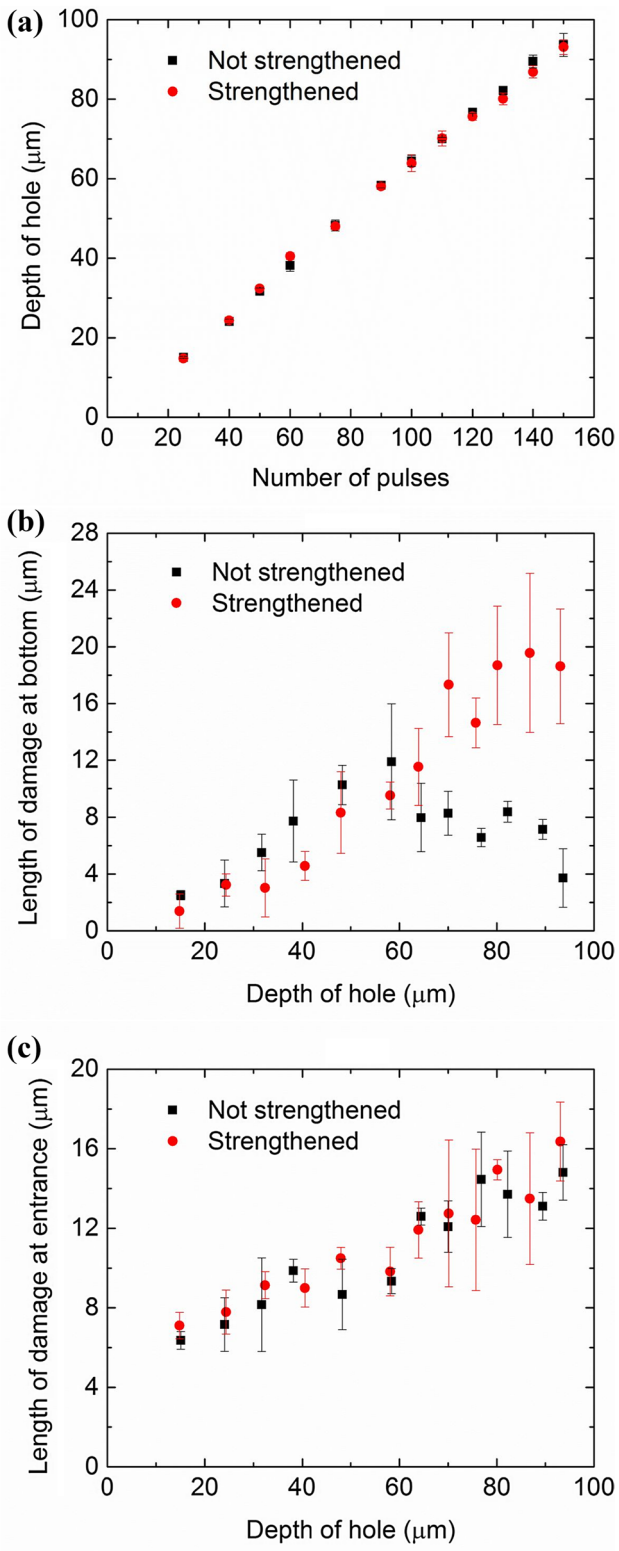

Fig. 3 **a** Dependence of the depth of a hole on the number of pulses. Dependence of damage length on the depth of a hole **b** at the bottom of the hole, and **c** at the entrance of the hole

damage length on the depth of a hole at the bottom of the hole and at the entrance of the hole are plotted in Fig. 3b and c, respectively. The horizontal axes in Fig. 3b, c correspond to the vertical axis in Fig. 3a. Figure 3b shows that the damage at the bottom of the hole in the strengthened glass is shorter than that of non-strengthened glass, until the hole depth reaches 60 μm. However, this tendency is reversed when the depth of the hole is larger than 60 μm. As the border between the regions of compressive and tensile stress in the strengthened glass is located at a depth of 62 μm, the data in Fig. 3b indicates that the damage formed at the bottom of the hole was caused by tensile stress. In addition, Fig. 3c shows that the length of damage at the entrance of the hole did not differ when drilling on strengthened glass and non-strengthened glass. This result indicates that the damage at the entrance of the hole was formed without being affected by a stress field.

3.2 Stress simulation

The damage around the sidewall and bottom of the hole was found to be affected by tensile stress, which may be present during the drilling of both strengthened and non-strengthened glasses. To investigate the mechanism behind the formation of the tensile stress during the drilling, we analyzed the stress wave propagating inside non-strengthened glass using the finite element method. The governing equation is an elasticity equation. During the analysis, we modeled a hole drilled by 75 laser pulses to investigate the distribution of stress generated inside a hole. The radius and height of the axisymmetric model were 50 and 100 μm, respectively, which were sufficiently large for this calculation. The motion in the horizontal direction at the outer edge of the model was constrained, and the motion in both the horizontal and vertical directions at the bottom of the model was constrained. The stress propagating inside a material is considered to be produced by a thermoelastic wave [11]. This thermoelastic wave is produced by an adiabatic expansion. However, the ejection of material occurs approximately at the same time as the stress starts to propagate inside the material [11, 19, 20]. Therefore, we assumed that the expansion involved a pressure load on the material and the ejection of the material, and that the impulse applied to the material is equal to the momentum of the ejected material, based on the conservation of momentum.

The volume removed by the 75th laser pulse was calculated to be 30.3 μm^3 by performing a simulation shown in references [18, 21]. We calculated the density of free electrons using the simulation and assumed that the energy density of atoms is equal to the product of the density of free electrons and band gap. In the calculation of the density of free electrons, we assumed that the number of free electrons per atom does not exceed the number of electrons

in the outermost shell of the atom. The energy is consumed as kinetic energy. Therefore, the average speed of the ejected material is expressed as $v = \sqrt{2E/m}$, where $E = 5.5$ μJ is the kinetic energy of the ejected material and $m = 7.6 \times 10^{-11}$ g is its mass. The pressure exerted on the material is expressed as $p = mv/(A\Delta t)$, where $A = 1.4$ μm^2 is the area at the bottom of a hole where the material is removed, and $\Delta t = 10$ ps is the time interval over which we assumed that the ejected material keeps pushing the surface of the hole. Initially, no pressure was loaded. Then, a pressure $p = 675$ GPa was loaded for 10 ps at the bottom of the hole. Figure 4a, b shows the illustration of model parameters and the mesh shape, respectively. The region where the pressure was loaded is shown by a red curve in Fig. 4a.

Figure 5 shows the results of the analysis of the stress distribution. The direction and the length of the arrows shown in the figures express the direction and the magnitude of the principal stress. Initially, the compressive stress is generated around the bottom of the hole, as shown in Fig. 5a, b. The results show that the surface where the pressure was loaded is pushed out and stretched 0.1 ns after loading the pressure. The stretch of the surface area indicates that the distance between the atoms is expanded in a circumferential direction at the bottom of the hole. However, at this moment, the atoms on the surface are compressed in the radial direction. Owing to the Poisson's effect caused by the compression, the atoms in a circumferential direction are compressed despite the surface being stretched. After the passage of compressive stress wave through the surface, the compression in the atoms on the surface is released. Therefore, a tensile stress is generated at the bottom of the hole 0.2 ns after loading the pressure, as shown in Fig. 5c, e. As this tensile stress is distributed in a circumferential direction on the surface of the bottom of the hole, the stress can facilitate crack initiation perpendicular to the curve of the bottom surface. In particular, during this process, the maximum tensile stress in a circumferential direction on the surface of the bottom of the hole reaches 8 GPa. This value is larger than the theoretical tensile strength of glass, which is calculated to be 6.6 GPa [22]. Furthermore, it is known that the actual tensile strength of glass is far below the theoretical strength [22]. Therefore, the tensile stress is large enough to cause cracks. As shown in Fig. 5d, the tensile-stress wave begins propagating inside the material 1 ns after loading the pressure. Consequently, the short cracks initiated on the surface can be elongated by following the propagating tensile stress, resulting in long cracks.

In the strengthened glass, the original compressive-stress field cancels the tensile stress caused by the shock. Contrarily, the original tensile-stress field enhances the effect of the tensile stress caused by the shock upon the generation of the cracks. In this manner, the differences in the damage lengths shown in Fig. 3b can be explained.

These results indicate that the microscopic damage observed at the bottom of the hole was caused by the stress wave generated by each laser pulse. The damage observed at the sidewall of the hole is considered to be the crack which is first generated at the bottom and then left inside the glass without being removed after the hole becomes deeper with continued application of multiple laser pulses.

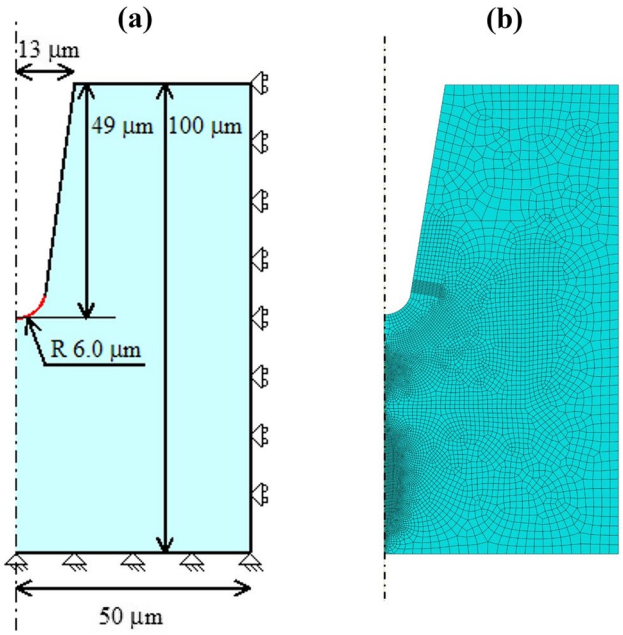

Fig. 4 **a** Illustration of model parameters. **b** Mesh shape

3.3 Temperature simulation

The damage at the entrance of the hole was formed without being affected by a stress field, as shown in Fig. 3c. This result indicates that the damage formed around the entrance was caused by a factor different from the tensile stress generated by the stress wave. As the factor of damage which is not caused by tensile stress, modification by heat can be considered [23–25]. To investigate the effect of heat on the damage formation, we calculated the temperature distribution while the processing of laser drilling was ongoing, based on the calculation of the distributions of the laser intensity and the free-electron density inside glass. The distribution of the intensity has been calculated using the beam propagation method [26]. The free-electron density ρ is calculated based on the rate equation:

$$\frac{\partial \rho}{\partial t} = \sigma I^k + \alpha_c I \rho - \eta_{\mathrm{rec}} \rho^2 - \eta_{\mathrm{diff}} \rho \tag{1}$$

where t is time, I is the intensity, k is the number of photons for multi-photon ionization, σ is the coefficient of multi-photon ionization, α_c is the coefficient of cascade ionization, η_{rec} is the coefficient of recombination, and η_{diff} is the

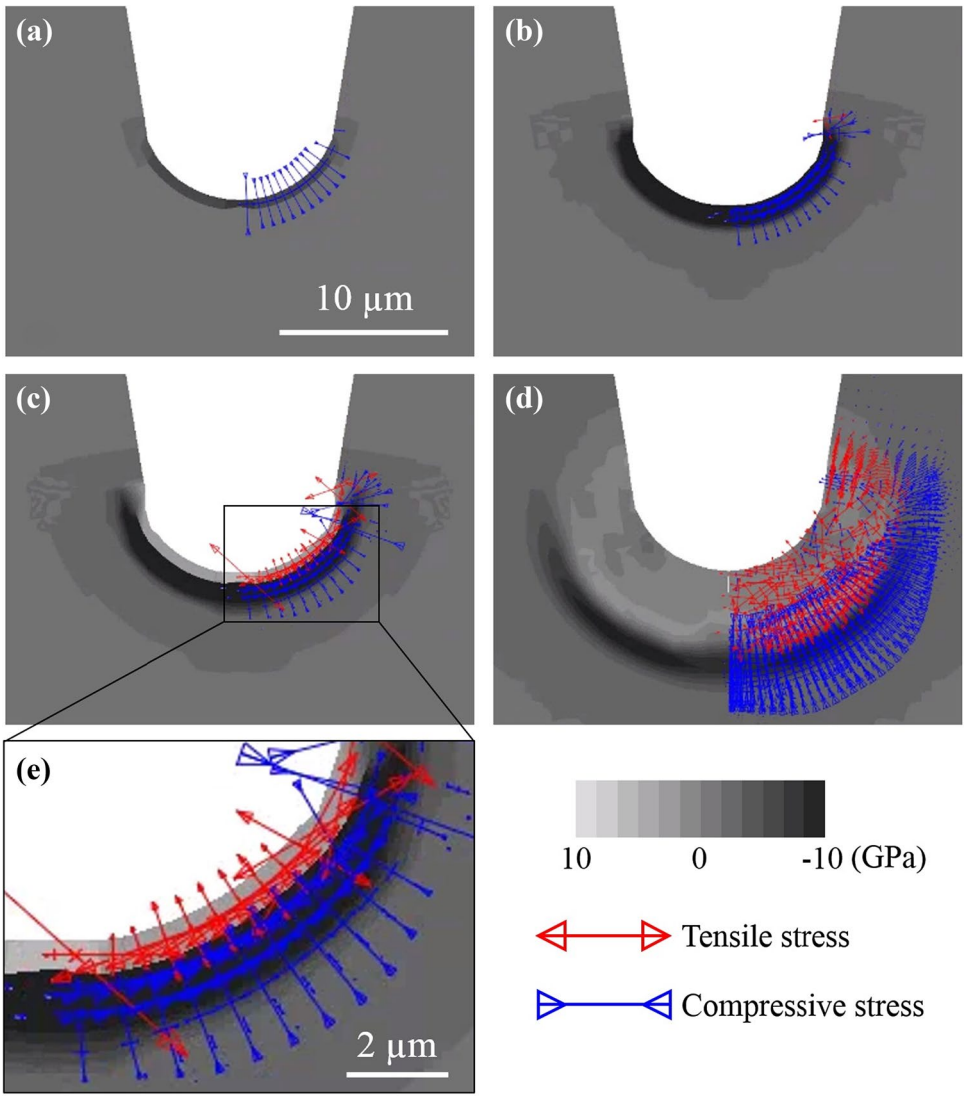

Fig. 5 Stress distribution at the bottom of a hole **a** 10 ps, **b** 0.1 ns, **c** 0.2 ns, and **d** 1 ns after the 75th laser pulse is shot. The enlarged view of (**c**) is shown in (**e**)

coefficient of diffusion [18, 27, 28]. Because the energy of the free electrons is transferred to phonons, the increase in temperature ΔT can be expressed as follows [29]:

$$\Delta T = \frac{E_{av}}{3nk_B} \int_0^\infty (\sigma I^k + \alpha_c I \rho) \mathrm{d}t \tag{2}$$

where E_{av} is the average electron energy, n is the number of atoms in a unit volume, and k_B is the Boltzmann constant [30]. Electrons and the lattice reach thermal equilibrium in less than 10 ps [31], and the heat capacity of electrons is much smaller than the heat capacity of the lattice. Therefore, it is appropriate to assume that the entire energy absorbed by electrons is given to the lattice, and is balanced by the increase in the lattice energy $3nk_B\Delta T$.

The distributions of intensity, free-electron density, and temperature are obtained by repeating the calculations with each laser pulse. To estimate the shape of the drilled hole, we assumed that the volume where the free-electron density was higher than the critical value or where the temperature was higher than the boiling point was removed. The estimated shapes are compared with the experimental results in Fig. 6. The conditions used in the calculation and experiments were the same.

The shape of the hole drilled by 75 laser pulses and the temperature distribution generated by the 75th laser pulse are shown in Fig. 7a. This result shows that high temperature is localized around the entrance of the hole. We defined a d-axis along the high-temperature region, which makes an angle of 19.8° with the optical axis as shown in Fig. 7b. The origin of the d-axis was set 1 µm away from the sidewall of the hole.

The localization of the high temperature along the d-axis was caused by the reinforcement of the electric field along the angle. The reinforcement of the electric field increases the density of the free electrons and results in the generation

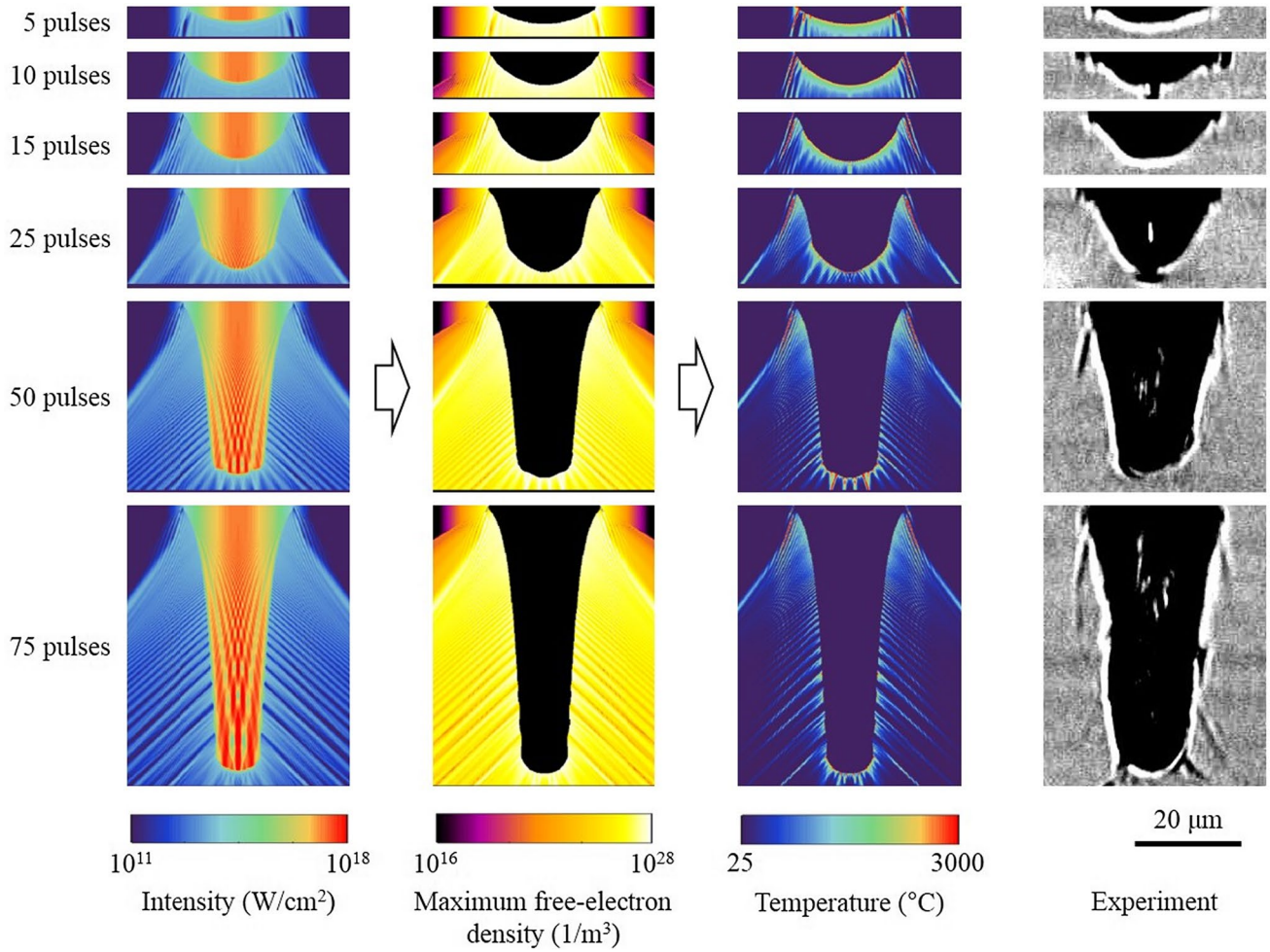

Fig. 6 Procedure for estimating the shape of the hole and temperature. The estimated shapes are compared with the experimental results

of heat. The angle of the d-axis is consistent with the angle of the damage observed after the experiment, which was 16.6°. This consistency indicates that the localization of high temperature may affect the generation of damage. To investigate the effect of the temperature increase on the damage generation, we evaluated the size of the region along the d-axis, where the residual strain is created. The time dependence of the temperature along the d-axis has been plotted in Fig. 7c.

The stress relaxation following the application of strain caused by the thermal expansion under high temperature is analyzed by a viscoelastic model [23, 32]. Using the simplest viscoelastic model (Maxwell element), the percentage of relaxation can be expressed as $P = 100\%[1 - \exp(-Kt/\eta)]$, where $K = 45.7$ GPa is the bulk modulus and η is the temperature-dependent viscosity [23]. Although the viscosity of glass changes drastically with changes in temperature, the change in the bulk modulus is much smaller. Therefore, the temperature and the time needed to achieve a certain percentage of relaxation can be calculated by assuming the viscosity being a function of temperature and the bulk modulus as a constant. Figure 7d shows the time needed for the stress to be 99.5% relaxed under different temperatures. This indicates that the stress can be relaxed in a short time under high-temperature conditions.

When the material is rapidly cooled down after the relaxation, the strain is confined inside the material. The region where the strain remains is observed as the modification [23]. To investigate the confinement of strain inside the material, we calculated the time dependence of the percentage of relaxation along the d-axis. Figure 8a shows the time dependence of the length of the region where the stress is over 99.5% relaxed along the d-axis. This indicates that the material between the origin of the d-axis and the position 6.4 µm away from the origin along the d-axis has experienced relaxation after the beam was incident. The time dependence of the temperature at the position of 6.4 µm on the d-axis has been compared with the relaxation curve, which indicates the time dependence of the temperature needed for 99.5% stress relaxation, as shown in Fig. 8b.

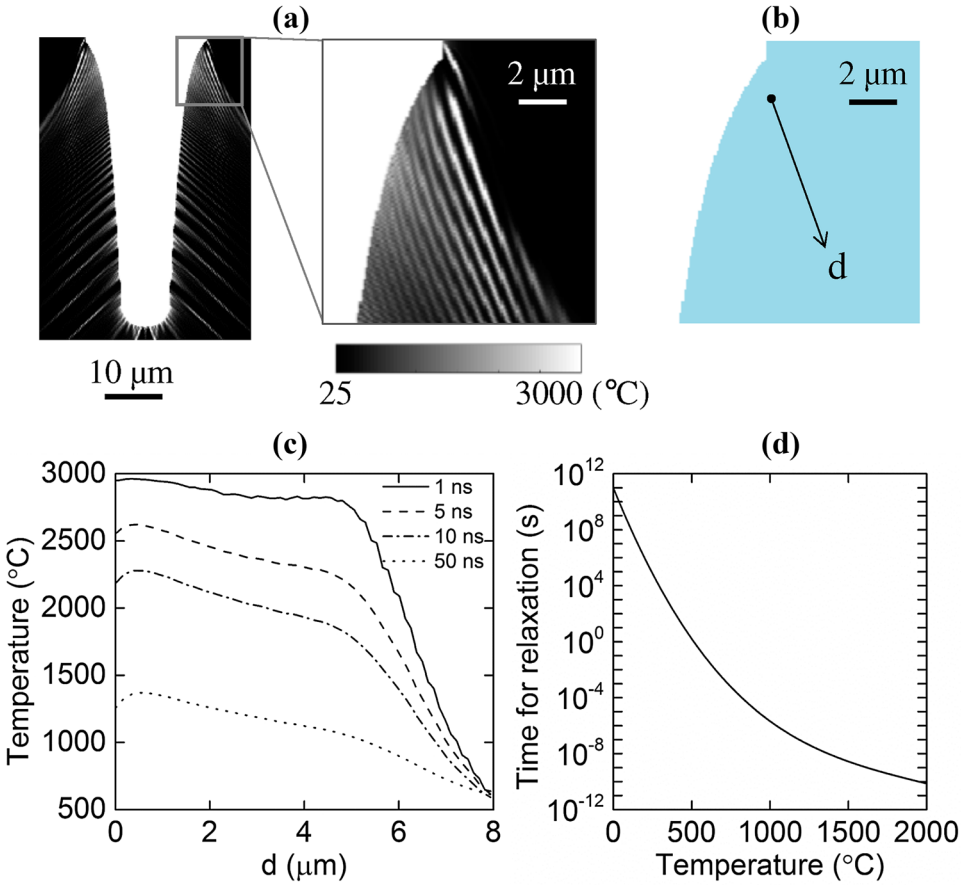

Fig. 7 **a** Temperature distribution around a hole generated by 75 laser pulses. **b** Illustration of the magnified view of the entrance of the hole and definition of the *d*-axis. **c** Temperature distribution along the *d*-axis. **d** Time needed for 99.5% stress relaxation under different temperatures

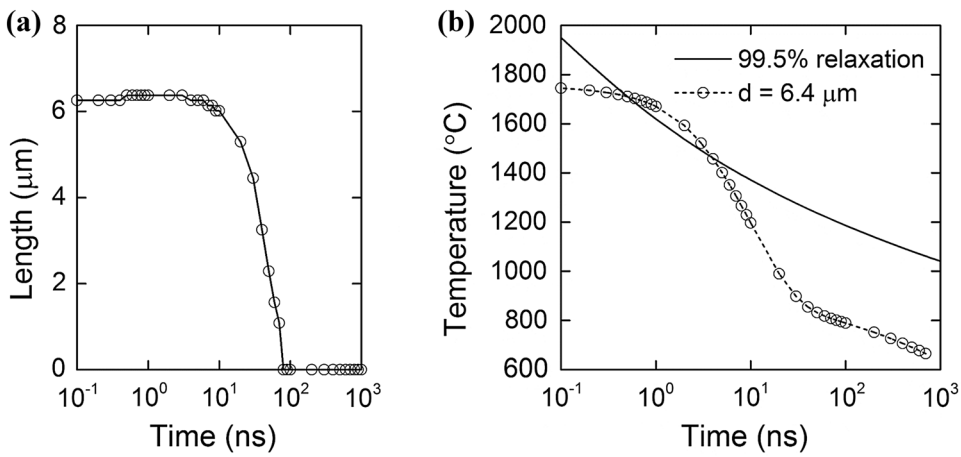

Fig. 8 **a** Time dependence of the length of the region where the percentage of stress relaxation is over 99.5% along the *d*-axis. **b** Time dependence of the temperature at 6.4 μm on the *d*-axis compared with the time dependence of the temperature needed for 99.5% stress relaxation

The temperature at this position is lower than the relaxation curve before 0.5 ns. This indicates that the exposure time for high temperature is not sufficient for the stress to be fully relaxed before 0.5 ns. After 0.5 ns, the temperature at the position reaches the temperature required for 99.5% stress relaxation, indicating that the stress is fully relaxed. However, after 4 ns, the temperature decreases rapidly by thermal conduction, following which the temperature again becomes lower than the relaxation curve. This result indicates that the strain generated during the relaxation process is confined to the material 4 ns after the beam fires and forms the modification. The calculated length of the modification (6.4 μm) is consistent with the length of the damage observed after the experiment (7.3 μm). This result indicates that the damage observed at the entrance of the hole is a modification generated by the stress relaxation due to the exposure to high

temperature followed by a rapid cooling process owing to thermal conduction.

4 Conclusion

In conclusion, we presented mechanisms of the formation of damage in femtosecond laser microdrilling, revealing that the damage at the sidewall and bottom of a generated hole is mainly due to the stress wave, while the damage around the hole entrance is mainly due to relaxation of thermal stress. In particular, we quantitatively showed the time courses of the passage of the stress wave and the temperature distribution generated by the excited electrons. This research would be useful in developing a strategy to inhibit the damage and improve the quality of micromachining. To reduce irregular microscopic cracks at the sidewall and bottom of a hole, we would develop a processing technique in which the tensile stress is canceled. To reduce modification at the entrance of the hole, we would optimize the laser parameters to avoid the localization of temperature increase or develop glass materials with high heat resistance.

Acknowledgements We would like to thank Mr. Marinho, Dr. Nakao, and Dr. Maruyama for their constructive discussions.

References

1. G.D. Valle, R. Osellame, P. Laporta, J. Opt. A: Pure Appl. Opt. **11**, 013001 (2009)
2. L. Ji, Y. Hu, J. Li, W. Wang, Y. Jiang, Appl. Phys. A **121**, 1163 (2015)
3. C.B. Schaffer, A. Brodeur, J.F. Garcia, E. Mazur, Opt. Lett. **26**, 93 (2001)
4. R.R. Gattass, E. Mazur, Nat. Photon. **2**, 219 (2008)
5. F. Chen, J.R.V. Aldana, Laser Photon. Rev. **8**, 251 (2014)
6. K.M.T. Ahmmed, C. Grambow, A.M. Kietzig, Micromachines **5**, 1219 (2014)
7. R. Shinomoto, Y. Ito, T. Kizaki, K. Tatsukoshi, Y. Fukasawa, K. Nagato, N. Sugita, M. Mitsuishi, Int. J. Autom. Tech. **10**, 863 (2016)
8. C.B. Schaffer, A. Brodeur, E. Mazur, Meas. Sci. Technol. **12**, 1784 (2001)
9. T. Sano, H. Mori, O. Sakata, E. Ohmura, I. Miyamoto, A. Hirose, K.F. Kobayashi, Appl. Surf. Sci. **247**, 571 (2005)
10. X. Zeng, X. Mao, S.S. Mao, S.B. Wen, R. Greif, R.E. Russo, Appl. Phys. Lett. **88**, 061502 (2006)
11. N. Zhang, X. Zhu, J. Yang, X. Wang, M. Wang, Phys. Rev. Lett. **99**, 167602 (2007)
12. D.M. Krol, J. Non. Cryst. Solids **354**, 416 (2008)
13. S. Panchatsharam, B. Tan, K. Venkatakrishnan, J. Appl. Phys. **105**, 093103 (2009)
14. M. Sakakura, T. Tochio, M. Eida, Y. Shimotsuma, S. Kanehira, M. Nishi, K. Miura, K. Hirao, Opt. Express **19**, 17780 (2011)
15. M. Sakakura, T. Okada, Y. Shimotsuma, N. Fukuda, K. Miura, J. Laser Micro. Nanoen. **10**, 320 (2015)
16. Y. Ito, T. Kizaki, R. Shinomoto, M. Ueki, N. Sugita, M. Mitsuishi, Precis. Eng. **47**, 498 (2017)
17. J.R. Vazquez de Aldana, C. Mendez, L. Roso, P. Moreno, J. Phys. D: Appl. Phys. **38**, 2764 (2005)
18. M. Sun, U. Eppelt, S. Russ, C. Hartmann, C. Siebert, J. Zhu, W. Schulz, Opt. Express **21**, 7858 (2013)
19. P. Lorazo, L.J. Lewis, M. Meunier, Phys. Rev. Lett. **91**, 225502 (2003)
20. X. Wang, X. Xu, J. Therm. Stresses **25**, 457 (2002)
21. U. Eppelt, S. Russ, C. Hartmann, M. Sun, C. Siebert, W. Schulz, ICALEO **31**, M504 (2012)
22. R.W. Davidge, *Mechanical behavior of ceramics, Ch 3* (Cambridge University, Cambridge, 1979)
23. M. Sakakura, M. Shimizu, Y. Shimotsuma, K. Miura, K. Hirao, Appl. Phys. Lett. **93**, 231112 (2008)
24. M. Shimizu, M. Sakakura, M. Ohnishi, Y. Shimotsuma, T. Nakaya, K. Miura, K. Hirao, J. Appl. Phys. **108**, 073533 (2010)
25. M. Shimizu, M. Sakakura, S. Kanehira, M. Nishi, Y. Shimotsuma, K. Hirao, K. Miura, Opt. Lett. **36**, 2161 (2011)
26. J.V. Roey, J.V.D. Donk, P.E. Lagasse, J. Opt. Soc. Am. **71**, 803 (1981)
27. P.K. Kennedy, IEEE J. Quant. Electron. **31**, 2241 (1995)
28. A. Vogel, J. Noack, G. Huttman, G. Paltauf, Appl. Phys. B **81**, 1015 (2005)
29. M. Sun, U. Eppelt, W. Schulz, J. Zhu, Opt. Mater. Express **3**, 1716 (2013)
30. N.W. Ashcroft, N.D. Mermin, *Solid State Physics, Ch 22* (Holt, Rinehart and Winston, New York, 1976)
31. T.Q. Qui, C.L. Tien, J. Heat Transfer **115**, 835 (1993)
32. A.K. Varshneya, *Fundamentals of inorganic glasses, Ch 13* (Academic, New York, 1994)